Robotica (2017) volume 35, pp. 1732–1746. © Cambridge University Press 2016
doi:10.1017/S0263574716000461

Industrial compliant robot bases in interaction tasks: a force tracking algorithm with coupled dynamics compensation

Loris Roveda*, Nicola Pedrocchi, Federico Vicentini and Lorenzo Molinari Tosatti

Institute of Industrial Technologies and Automation (ITIA) of Italian National Research Council (CNR), via Bassini, 15 - 20133 Milan, Italy. E-mails: nicola.pedrocchi@itia.cnr.it, federico.vicentini@itia.cnr.it, lorenzo.molinari@itia.cnr.it

(Accepted June 11, 2016. First published online: July 7, 2016)

SUMMARY
Light-weight manipulators are used in industrial tasks mounted on mobile platforms to improve flexibility. However, such mountings introduce compliance affecting the tasks. This work deals with such scenarios by designing a controller that also takes into account compliant environments. The controller allows the tracking of a target force using the estimation of the environment stiffness (EKF) and the estimation of the base position (KF), compensating the robot base deformation. The closed-loop stability has been analyzed. Observers and the control law have been validated in experiments. An assembly task is considered with a standard industrial non-actuated mobile platform. Control laws with and without base compensation are compared.

KEYWORDS: Interaction control; Model based control; Compliant robot base compensation; Impedance control; Industrial robotics.

1. Introduction

Light-weight manipulators have been increasingly used in interacting robotic tasks in which reduced manipulator mass and high (controlled) compliance are required in order to ensure safety and adaptability during the task execution. Focused tasks include industrial applications (e.g., automatic assembly, cooperative disassembly, handling assistance and machining processes), in which manipulators share the same working area with other manipulators and human operators, while interacting with a compliant and (partially) unknown environment. Moreover, lightweight manipulators are often mounted on flexible structures or mobile platforms. In such applications, the dynamics of the interaction during the task execution is affected by both the interacting ports.[1,2]

1.1. Interaction control: Related works

The principal methods for accomplishing robust and safe interactions certainly involve compliance controls. Since the beginning of sensor-based force/dynamics control,[3–7] dynamic balance between controlled robots and environments have been primarily followed the approach of impedance control,[8] also including non-restrictive assumptions[9] on the dynamical properties of the environment. Nevertheless, some force/deformation regulation requirements have been introduced (investigated, designed and validated) in order to improve the robustness and safety of interaction with a dynamic task, especially in the case of a precision-force process.[10] Although impedance methods are proved to be dynamically equivalent to explicit force controllers,[11] a direct tracking of explicit interaction forces or deformation is not straightforwardly allowed. To overcome this limitation to preserve the properties of the impedance behavior, two different families of methods have been mainly introduced: class (a) force-position tracking impedance controllers[12–15] and class (b) variable impedance controllers.[16,17]

* Corresponding author. E-mail: loris.roveda@itia.cnr.it

Class (a) methods have been considered as a starting point to develop the control strategy described in this paper. Therefore, such class of controllers is described in the following Section.

1.1.1. Force-position tracking impedance control. The force/position-tracking impedance control family have been designed in order to straightforwardly track a force (or position) reference $\mathbf{f}^d$ (or $\boldsymbol{x}^0$) using impedance control.

Many efforts have been made to achieve such force (or position) tracking with impedance control despite the lack of knowledge of the environmental stiffness and location,[12] usual conditions for impedance control applications, in which the controlled force is derived from a position control law, by scaling the trajectory as a function of the estimated environment stiffness and calculating the time-varying PID gains. Another important approach[13–15] involves the generation of a reference motion as a function of the force-tracking error, under the condition that the environment stiffness is variously unknown, i.e., estimated as a function of the measured force.

The limitations of such class of control strategies are related to force overshoots and limited bandwidth of the controllers, which implies instabilities related to the variation of the environment stiffness.

1.1.2. Compliant robot base dynamics compensation in interaction control. The compensation of the compliant robot base dynamics has been widely investigated in order to improve performance in both free-motion[18–21] and interacting tasks.[22–24]

Some works are aimed at assigning explicit values to such relationship in the case of gravitation-free application,[18] or in the case of standard gravitation load in order to highlight the influence of the single terms on the coupled-system dynamics.[19] Some works are focused on flexible structure mounted manipulator systems aiming at developing a control method to avoid base vibration.[20] Introduces a dynamic analysis for reaction management control using the Reaction Null Space, while[21] considers a direct measurement of the base oscillation as a feedback to modulate the manipulator actuator input.

Similar explicit/feedback approaches have also been extended to interaction tasks. In ref. [22] contact force control of a flexible long-reach micro/macromanipulator is discussed. The proposed algorithm smooths the manipulator's transition from a free-space motion to the contact with an unknown environment. Moreover, impedance control-based algorithms considering known[23] or bounded[24] base stiffness have been investigated in order to return the manipulator stiffness to the desired one.

The limitations of the described strategies are related to the fact that several algorithms do not consider the interacting tasks and the use of external sensors is required (i.e., using signals as feedback) to implement the control algorithms (which is a critical issue, especially within the industrial context).

1.2. Paper contribution

In this paper, a control algorithm is defined for applications in which a light-weight manipulator with compliant mounting base (a KUKA LWR 4+ has been used) interacts with compliant environments of (partially) unknown geometrical and mechanical properties. Being based on the force-tracking impedance control, the algorithm is defined (i) to compensate for the base robot dynamics, (ii) by estimating the base deformation and the environment dynamical properties in order (iii) to set a pose reference for the impedance controller for force-tracking applications.

An Extended Kalman Filter (EKF) is implemented in order to estimate the environments parameters, while a Kalman Filter (KF) is implemented in order to estimate the robot base position (which is based on a regular off-line model identification) and this has been used as a feedback to avoid the use of external sensors. The control strategy has been validated in experiments that involve an assembly task. A constant environment stiffness and a compliant base stiffness have been considered as validation set-up. In particular, a compliant fixed environment and a standard industrial non-actuated mobile platform have been considered, as shown in Section 5. The proposed strategy has been compared with a classical force tracking impedance controller without robot base dynamic compensation.

2. Interaction Dynamics

2.1. Controlled robot dynamics

The internal loop has been designed with the purpose of achieving a pure decoupled second-order impedance behavior for the controlled robot up to a reasonable frequency around 5 Hz. Such behavior can be achieved by properly designing a control loop around the standard position controller for many

https://doi.org/10.1017/S0263574716000461 Published online by Cambridge University Press

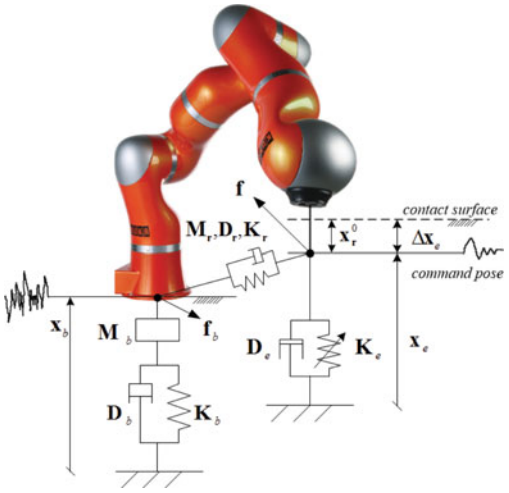

Fig. 1. Coupled system robot base – controlled robot – interacting environment.

lightweight industrial robots. Therefore, the target dynamics for the controlled robot should result in

$$\mathbf{M}_r\ddot{\mathbf{x}}_r + \mathbf{D}_r\dot{\mathbf{x}}_r + \mathbf{K}_r\Delta\mathbf{x}_r = \mathbf{f}_r, \quad \text{with} \quad \Delta\mathbf{x}_r := \mathbf{x}_r - \mathbf{x}_r^0, \tag{1}$$

where $\mathbf{x}_r^0$ and $\mathbf{x}_r$ are the desired and current robot positions, respectively, and $\mathbf{f}_r$ is the external interacting force/torque (Fig. 1). In addition, the Cartesian stiffness $\mathbf{K}_r$, damping $\mathbf{D}_r$ and mass $\mathbf{M}_r$ have to present negligible/irrelevant extra-diagonal coupling terms with a good approximation up to a few Hz.

Remarkably, the KUKA LWR4+, that is the robot used for the experimental tests, already displays such behavior of ref. [25]. In fact, experiments show that also $\mathbf{M}_r$ presents negligible/irrelevant extra-diagonal coupling terms with a good approximation up to 5 Hz.[26]

2.2. *Compliant environment dynamics*

Under the hypothesis that exchanged forces remain unaltered at the interaction point, i.e., $\mathbf{f}_e = \mathbf{f}_r = \mathbf{f}$ (where $\mathbf{f}_e$ is the interaction force acting on the environment due to the robot action), the simplest way to describe the environment dynamics is the linear KelvinVoigt contact model[27] (mass $\mathbf{M}_e$ - spring $\mathbf{K}_e$ - damper $\mathbf{D}_e$ model[28,29]), given the environment equilibrium position $\mathbf{x}_e^{eq}$.

Considering soft environments, diagonally dominant natural frequencies could display resonances in the operating bandwidth of the linearly decoupled impedance control. This could result in undesired oscillations of the environment that could hinder the stability of the task execution. However, taking into consideration a reasonable task bandwidth limited at 5Hz, the worst case – e.g., undamped – minimum ratio $\min_i \frac{K_e}{M_e}$, $\forall i$ DoFs, is about $15^2 \frac{N^2}{m^2\text{kg}^2}$, so that in the damped case the masses of the environment model can be neglected. Accordingly, the environment pure impedance model results in

$$\sum_i (\mathbf{D}_e^i\dot{\mathbf{x}}_e^i + \mathbf{K}_e^i\Delta\mathbf{x}_e^i) = \mathbf{f}_e, \ \forall i = 1, \ldots, N, \tag{2}$$

where $\Delta\mathbf{x}_e^i = \mathbf{x}_e^i - \mathbf{x}_e^{eq,i}$, for all the finite number N of interaction points.

2.3. *Compliant robot base dynamics*

A compliant robot base can be modeled considering its relevant N eigenmodes in the target bandwidths. Considering the target low frequencies bandwidth, a simple mass $\mathbf{M}_b$ – spring $\mathbf{K}_b$ – damper $\mathbf{D}_b$ model is taken into account to describe the robot base dynamics[30]

$$\mathbf{M}_b\ddot{\mathbf{x}}_b + \mathbf{D}_b\dot{\mathbf{x}}_b + \mathbf{K}_b\Delta\mathbf{x}_b = \mathbf{f}_b, \tag{3}$$

https://doi.org/10.1017/S0263574716000461 Published online by Cambridge University Press

where $\mathbf{f}_b$ is the propagation of the interaction force from the robot end-effector to the compliant robot base.

2.4. Coupled dynamics

The coupled system dynamics has been defined by taking into account the absolute position $\mathbf{x}_b$ of the compliant robot base and the relative position of the robot $\mathbf{x}_r$ with respect to $\mathbf{x}_b$ as DoFs (i.e., the environment position results in $\mathbf{x}_e = \mathbf{x}_b + \mathbf{x}_r$). This is valid if considering translational DoFs, that is the main purpose of the presented work. Moreover, under the hypothesis that exchanged forces at interaction points remain unaltered, considering a single contact point, the resulting dynamics is (Fig. 1)

$$\begin{cases} 0 = \mathbf{M}_r(\ddot{\mathbf{x}}_r + \ddot{\mathbf{x}}_b) + \mathbf{D}_r\dot{\mathbf{x}}_r + \mathbf{K}_r(\mathbf{x}_r - \mathbf{x}_r^0) + \mathbf{D}_e\left(\dot{\mathbf{x}}_b + \dot{\mathbf{x}}_r\right) + \mathbf{K}_e\left(\mathbf{x}_b + \mathbf{x}_r - \mathbf{x}_e^{eq}\right), \\ 0 = \mathbf{M}_r(\ddot{\mathbf{x}}_r + \ddot{\mathbf{x}}_b) + \mathbf{M}_b\ddot{\mathbf{x}}_b + \mathbf{D}_b\dot{\mathbf{x}}_b + \mathbf{D}_e\left(\dot{\mathbf{x}}_b + \dot{\mathbf{x}}_r\right) + \mathbf{K}_b\mathbf{x}_b + \mathbf{K}_e\left(\mathbf{x}_b + \mathbf{x}_r - \mathbf{x}_e^{eq}\right). \end{cases} \tag{4}$$

3. Observers Design

3.1. Compliant environment observer: Extended Kalman filter

Due to the unknown/partially known geometry of a generic interacting environment, the model of the N interaction points as used in ref. [31] happens to be unfeasible. The environment in (2) is reduced to a translational lumped impedance model with diagonal $\mathbf{K}_e$ and $\mathbf{D}_e$ matrices to be used in the EKF dynamics.[32] Under the mild hypothesis that the contact is preserved once that it is established and that the contact(s) are elastic the robot-environment interaction is defined by the filter state, augmented with the environment properties

$$\boldsymbol{\xi}_e = [\Delta\mathbf{x}_e, \mathbf{K}_e, \mathbf{D}_e, \mathbf{f}_e]^T. \tag{5}$$

By substituting the augmented state (5) in model (2), the filter dynamics results in

$$\boldsymbol{f}(\boldsymbol{\xi}_e, \boldsymbol{\nu}_e) = \begin{bmatrix} \mathbf{D}_e^{-1}\left(-\mathbf{K}_e\Delta\mathbf{x}_e + \mathbf{f}_e + \boldsymbol{\nu}_{\mathbf{x}_e}\right) \\ \boldsymbol{\nu}_{\mathbf{K}_e} \\ \boldsymbol{\nu}_{\mathbf{D}_e} \\ \boldsymbol{\nu}_{\mathbf{f}_e} \end{bmatrix}, \tag{6}$$

where the vector $\boldsymbol{\nu}_e = [\boldsymbol{\nu}_{\mathbf{x}_e}, \boldsymbol{\nu}_{\mathbf{K}_e}, \boldsymbol{\nu}_{\mathbf{D}_e}, \boldsymbol{\nu}_{\mathbf{f}_e}]^T$ accounts for uncertainties in model parameters/estimates.

The observer of the augmented state is therefore defined as

$$\begin{cases} \widehat{\dot{\boldsymbol{\xi}}}_e = \boldsymbol{f}\left(\widehat{\boldsymbol{\xi}}_e, \boldsymbol{\nu}_e\right) + \mathbf{K}_{EKF}(\mathbf{y} - \mathbf{C}_a\widehat{\boldsymbol{\xi}}_e) \\ \widehat{\mathbf{y}} = \boldsymbol{h}\left(\widehat{\boldsymbol{\xi}}_e, \boldsymbol{w}\right) \end{cases}. \tag{7}$$

Based on,[32] the state $\widehat{\boldsymbol{\xi}}_e$ is updated by measurements of $\mathbf{x}_e$ and $\mathbf{f}_e = \mathbf{f}$, providing the environment stiffness $\widehat{\mathbf{K}}_e$.

$\widehat{\boldsymbol{\xi}}_e$ are estimates, $\mathbf{K}_{EKF}$ is the gain matrix

$$\mathbf{K}_{EKF} = \mathbf{P}\mathbf{C}_a\mathbf{R}^{-1}, \tag{8}$$

with $\mathbf{C}_a$ as the observation matrix, and $\mathbf{R}$ as the covariance measurement noise matrix defined as

$$\mathbf{R} = \mathbf{H}E\{\mathbf{w}\mathbf{w}^T\}\mathbf{H}^T = \mathbf{H}\mathbf{W}\mathbf{H}^T, \tag{9}$$

https://doi.org/10.1017/S0263574716000461 Published online by Cambridge University Press

where the observation function $\mathbf{h}$ linearly maps the sample inaccuracies, due to measurement noise $\mathbf{w}$, through the matrix $\mathbf{H}$

$$\mathbf{H} = \left.\frac{\partial \mathbf{h}}{\partial \mathbf{w}}\right|_{\widehat{\boldsymbol{\xi}}_e}. \tag{10}$$

The covariance matrix $\mathbf{P}$ and its rate, as in

$$\dot{\mathbf{P}} = \mathbf{A}_a\mathbf{P} - \mathbf{P}\mathbf{C}_a^T\mathbf{R}^{-1}\mathbf{C}_a\mathbf{P} + \mathbf{G}_a\mathbf{Q}\mathbf{G}_a^T + \mathbf{P}\mathbf{A}_a^T, \tag{11}$$

are based on the dynamics of the state and the model uncertainties, defined with matrix $\mathbf{A}_a$ and matrix $\mathbf{G}_a$, respectively

$$\mathbf{A}_a = \left.\frac{\partial \mathbf{f}}{\partial \mathbf{x}_a}\right|_{\widehat{\boldsymbol{\xi}}_e} \qquad \mathbf{G}_a = \left.\frac{\partial \mathbf{f}}{\partial \boldsymbol{\nu}_a}\right|_{\widehat{\boldsymbol{\xi}}_e}, \tag{12}$$

and on matrix $\mathbf{Q}$ used for the estimation of the parameters, which is defined as:

$$\mathbf{Q} = \mathbf{G}_a E\{\boldsymbol{\nu}\boldsymbol{\nu}^T\}\mathbf{G}_a^T = \mathbf{G}_a\mathbf{V}\mathbf{G}_a^T. \tag{13}$$

Vector $\mathbf{w} = [\mathbf{w}_p,\ \mathbf{w}_f]^T$ is based on an analysis of the noise content in the signal of position and force measurements. In particular $w_{p_i} = 10^{-3}$ and $w_{f_i} = 10^{-1}$ (where i indicates the $i-th$ degree of freedom) are the noise scalar values for position and force sampling, correspondingly replicated for all applied DoFs. Vector $\boldsymbol{\nu}$ is defined from experimental tests. In particular $\nu_{\mathbf{x}_{ei}} = 10^2$, $\nu_{\mathbf{K}_{ei}} = 10^6$, $\nu_{\mathbf{D}_{ei}} = 10^5$, $\nu_{\mathbf{f}_{ei}} = 10^2$, correspondingly replicated for all the applied DoFs.

3.2. Compliant robot base bbserver: Kalman filter

In order to avoid the use of external sensors (due to practical industrial considerations), on the basis of the compliant robot base dynamic model defined in (3), a KF[32] is used to estimate the position of the compliant robot base during the task execution. The compliant robot base dynamics is defined by the filter state, augmented with the interacting force

$$\boldsymbol{\xi}_b = [\dot{\mathbf{x}}_b,\ \Delta\mathbf{x}_b,\ \mathbf{f}_b]^T. \tag{14}$$

By substituting the augmented state (14) in model (3) the filter dynamics results in:

$$\boldsymbol{f}(\boldsymbol{\xi}_b, \boldsymbol{\nu}_b) = \begin{bmatrix} \widehat{\mathbf{M}}_b^{-1}\left(-\widehat{\mathbf{D}}_b\dot{\mathbf{x}}_b - \widehat{\mathbf{K}}_b\Delta\mathbf{x}_b + \mathbf{f}_b + \boldsymbol{\nu}_{\mathbf{x}_b}\right) \\ \boldsymbol{\nu}_{\dot{\mathbf{x}}_b} \\ \boldsymbol{\nu}_{\mathbf{f}_b} \end{bmatrix}, \tag{15}$$

where the vector $\boldsymbol{\nu}_b = [\boldsymbol{\nu}_{\dot{\mathbf{x}}_b},\ \boldsymbol{\nu}_{\mathbf{x}_b},\ \boldsymbol{\nu}_{\mathbf{f}_b}]^T$ accounts for uncertainties in models parameters/estimates, and $\widehat{\mathbf{M}}_b$, $\widehat{\mathbf{D}}_b$, $\widehat{\mathbf{K}}_e$ are the parameters of the full linear model in Eq. (3) identified off-line.

Based on,[32] the state $\widehat{\boldsymbol{\xi}}_b$ is updated by measurements of $\mathbf{f}_b = \mathbf{f}$, providing the base displacement $\mathbf{x}_b$.

The same procedure shown in Section 3.1 has been followed to perform the estimation, by choosing the vector $\mathbf{w} = \mathbf{w}_f$ on the basis of an analysis of the noise content in the signal of force measurements. In particular $w_{f_i} = 10^{-1}$ is the noise scalar values force sampling, correspondingly replicated for all the applied DoFs. Vector $\boldsymbol{\nu}$ is defined from experimental tests. In particular, $\nu_{\dot{\mathbf{x}}_{b_i}} = 10$, $\nu_{\mathbf{x}_{b_i}} = 10^2$, $\nu_{\mathbf{f}_{b_i}} = 10^4$, correspondingly replicated for all the applied DoFs.

3.3. Compliant robot base observer off-line estimation: FRF identification

The on-line estimation of the base position relies on previous knowledge of the dynamic parameters of the mounting. Model parameters have been obtained using a regular identification procedure on

https://doi.org/10.1017/S0263574716000461 Published online by Cambridge University Press

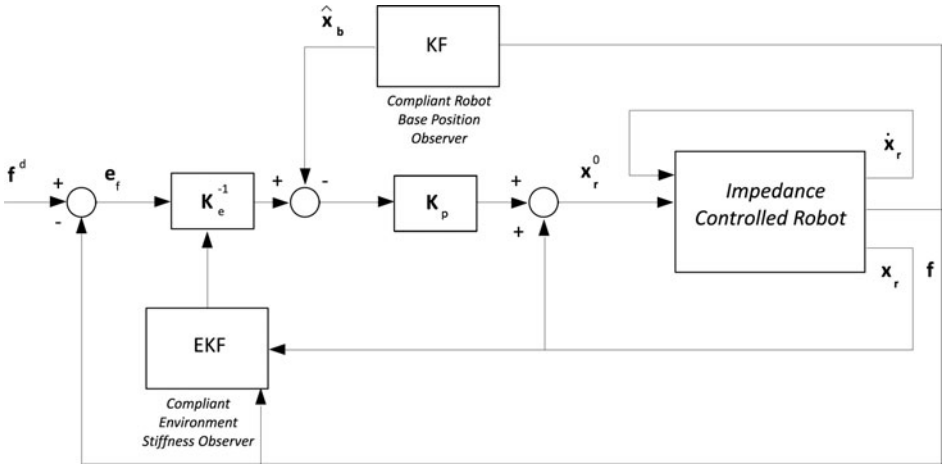

Fig. 2. Control flow-chart for a force-tracking ($\mathbf{f}^d$) application considering $\mathbf{K}_p^f = \mathbf{K}_p^b = \mathbf{K}_p$. The off-line identification of base parameters($\widehat{\mathbf{M}}_b$, $\widehat{\mathbf{D}}_b$, $\widehat{\mathbf{K}}_b$) provides the on-line estimation (KF) of the base deformation ($\mathbf{x}_b$) to compensate it.

motion data (i.e., accelerations) sampled[(1)] at the base during an auto-excitation provided by the robot in a given configuration. The pattern is a logarithmic $[0 - 10]$ Hz chirp of the end-effector pose along all the three translational and the three rotational axes, with an amplitude of 5 mm. The total chirp duration is 200 s and the reference pose of the robot is updated every 5 ms. Robot pose measurement (for force projection) is updated at 200 Hz, accelerations at 2000 Hz. The base model is evaluated through a modal analysis, defining the Frequency Response Functions (FRFs)[33] of the base system between commanded robot poses and measured accelerations.

4. Methodology

4.1. Control law

The force-tracking impedance control (Fig. 2) has been realized defining a target contact force $\mathbf{f}^d$ pattern acting on the environment during the execution of the task, dynamically forwarded as a pose(-velocity) reference $\mathbf{x}_r^0$. The designed control law aims at enabling the compensation of the base compliance, on-line estimating the environment stiffness and the robot base position to be used in the control algorithm

$$\mathbf{x}_r^0 = \mathbf{x}_r + \mathbf{K}_{p,f}\widehat{\mathbf{K}}_e^{-1}\mathbf{e}_f - \mathbf{K}_{p,b}\widehat{\mathbf{x}}_b, \tag{16}$$

$$\mathbf{e}_f = \mathbf{f}^d - \mathbf{f}_r, \tag{17}$$

$$\widehat{\mathbf{K}}_e = g_{EKF}(\mathbf{f}_e, \mathbf{x}_e^{eq}, \mathbf{x}_e), \tag{18}$$

$$\widehat{\mathbf{x}}_b = g_{KF}(\widehat{\mathbf{M}}_b, \widehat{\mathbf{D}}_b, \widehat{\mathbf{K}}_b, \mathbf{f}_b), \tag{19}$$

$\mathbf{K}_{p,f}$ and $\mathbf{K}_{p,b}$ are the proportional gains related to the force error and to the robot base position compensation. Dynamics parameters of the base $\widehat{\mathbf{M}}_b$, $\widehat{\mathbf{D}}_b$, $\widehat{\mathbf{K}}_b$ have been identified off-line (Fig. 2) and assumed to be constant along the task execution. The base compliance compensation is therefore two-fold: it recovers the dynamics response of the equivalent robot impedance behavior w.r.t. the environment (see Eqs. (16), (17)) and it enables the estimation of the environment stiffness, that is mandatory for expressing the tracking of $\mathbf{f}^d$ as a motion term in the impedance model (see Eqs. (16)–(18)).

[(1)]Accelerometers are only needed for the dynamic parameters identification procedure, not in the control loop.

https://doi.org/10.1017/S0263574716000461 Published online by Cambridge University Press

Remark 1. The main task space impedance loop has been performed by the model-based control of the manipulator at a rate of 200 Hz, synchronously with the environment estimation and with the robot base position estimation. Signals have been updated to the main KUKA LWR control loop, together with the sampling of force and kinematics state. The remote controller is based on a real-time Linux Xenomai platform with RTNet-patched network interfaces.

4.2. Closed-loop dynamics and stability

Considering a single contact point and a single degree of freedom for the clarity of presentation, the Laplace domain expression of the system in Eq. (4) is:

$$\begin{cases} 0 = \left[M_r s^2 + (D_e + D_r)s + (K_e + K_r)\right] X_r(s) + \left[M_r s^2 + D_e s + K_e\right] X_b(s) - K_r X_r^0(s), \\ 0 = \left[(M_r + M_b)s^2 + (D_e + D_b)s + (K_e + K_b)\right] X_b(s) + \left[M_r s^2 + D_e s + K_e\right] X_r(s), \end{cases} \tag{20}$$

under the hypothesis that dynamic parameters are either constant or varying at low rate (at least one decade lower than the response of the controlled system). The most notable of such cases is a time-varying stiffness of the environment K_e due to loading and process conditions.

The control law in Eq. (16) becomes

$$X_r^0(s) = X_r(s) + K_{p,f} \frac{E_f(s)}{K_e} - K_{p,b} X_b(s). \tag{21}$$

From the system dynamics in Eq. (20), transfer functions $T_1(s)$ and $T_2(s)$ can be derived between the robot or base position, respectively, and the reference control position in order to analyze the system stability

$$T_1(s) = \frac{X_r(s)}{X_r^0(s)} = + \frac{a_{12}s^2 + a_{11}s + a_{10}}{b_{14}s^4 + b_{13}s^3 + b_{12}s^2 + b_{11}s + b_{10}}, \tag{22a}$$

$$T_2(s) = \frac{X_b(s)}{X_r^0(s)} = - \frac{a_{22}s^2 + a_{21}s + a_{20}}{b_{24}s^4 + b_{23}s^3 + b_{22}s^2 + b_{21}s + b_{20}}, \tag{22b}$$

where

$$\begin{aligned} a_{12} &= M_b K_r + M_r K_r \\ a_{11} &= D_b K_r + D_e K_r \\ a_{10} &= K_b K_r + K_e K_r \\ b_{14} &= M_b M_r \\ b_{13} &= M_b D_e + M_r D_b + M_b D_r + M_r D_r \\ b_{12} &= M_b K_e + M_r K_b + M_b K_r + M_r K_r + D_b D_e + D_b D_r + D_e D_r \\ b_{11} &= D_b K_e + D_e K_b + D_b K_r + D_r K_b + D_e K_r + D_r K_e \\ b_{10} &= K_b K_e + K_b K_r + K_e K_r \end{aligned} ,$$

and

$$\begin{aligned} a_{22} &= M_r K_r \\ a_{21} &= D_e K_r \\ a_{20} &= K_e K_r \\ b_{24} &= M_b M_r \\ b_{23} &= M_b D_e + M_r D_b + D_r M_b + M_r D_r \\ b_{22} &= M_b K_e + M_r K_b + M_b K_r + M_r K_r + D_b D_e + D_b D_r + D_e D_r \\ b_{21} &= D_b K_e + D_e K_b + D_b K_r + D_r K_b + D_e K_r + D_r K_e \\ b_{20} &= K_b K_e + K_b K_r + K_e K_r \end{aligned} ,$$

$T_1(s)$ and $T_2(s)$ do not depend on control gains $K_{p,f}$ and $K_{p,b}$, which are instead factors of the transfer function $R(s)$ between the force error $E_f(s)$ and the reference $X_r^0(s)$ derived from the control

https://doi.org/10.1017/S0263574716000461 Published online by Cambridge University Press

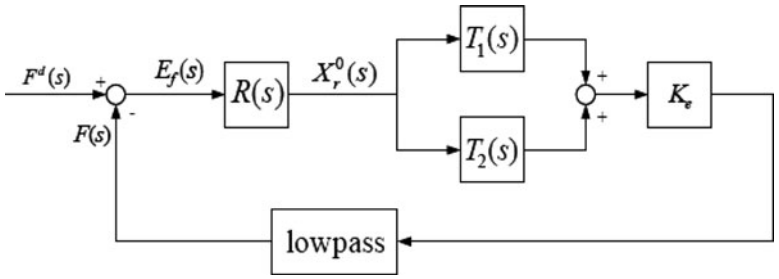

Fig. 3. Closed-loop control scheme with compound transfer functions and low-pass filter on the force feedback.

Eq. (21)

$$R(s)^{-1} = \frac{E_f(s)}{X_r^0(s)} = \frac{K_e}{K_{p,f}} - T_1(s)\frac{K_e}{K_{p,f}} + T_2(s)\frac{K_e K_{p,b}}{K_{p,f}}. \tag{23}$$

The transfer functions (22) and (23) constitute the control scheme in Fig. 3, where two closed-loop transfer functions $L_1(s)$ and $L_2(s)$ are defined

$$L_1(s) = \frac{R(s)T_1(s)K_e}{D_f(s) + (R(s)T_1(s)K_e)}, \tag{24}$$

$$L_2(s) = \frac{R(s)T_2(s)K_e}{D_f(s) + (R(s)T_2(s)K_e)}, \tag{25}$$

between the reference force $F^d(s)$ and the force acting on either the robot end-effector ($F(s)$) or the robot base ($F_b(s)$), respectively. $D_f(s)$ is a low pass filter (second order damped IIR filter, cut frequency 5 Hz) introduced to take into account the filtering effects on force readings from the LWR platform.

$L_1(s)$ and $L_2(s)$ have been used to validate the stability of the control system w.r.t. the control gains $K_{p,ef}$ and $K_{p,b}$ applied to the problem of rejecting the tracking force error $E_f(s)$.

By analyzing the transfer functions $L_1(s)$ and $L_2(s)$, it is possible to define a map of the optimal gains $K^\star_{p,f}$ and $K^\star_{p,b}$ that maximize the controller performance as a function of the system stiffnesses configuration. The $K^\star_{p,ef}$ is the value of $K_{p,ef}$ to be set in order to avoid instabilities with the constraint of obtaining the force tracking performance with null steady-state error (Fig. 4(a)). Given such value, the maximum gain $K^\star_{p,b}$ has also been set (Fig. 4(b)).

Remark 2. A table of the optimal gains is created on the base of on the coupled dynamics parameters in order to select the proper gains values during the task execution. The estimated environment stiffness is continuously updated and communicated to the controller and the proper gains have been selected.

Remark 3. The optimal control gains $K^\star_{p,ef}$ and $K^\star_{p,b}$ are defined in order to properly track the target interaction during the task execution (i.e., zero steady state error). Nevertheless, small errors in the estimates of the coupled parameters defined in Section 3 result in a non-optimal control gains selection. However, closed-loop stability is preserved if the parameters estimation is sufficiently accurate (i.e., the order of magnitude of the estimated parameters corresponds to the order of magnitude of the real parameters) but the tracking performance will be affected (i.e., non-zero steady state error).

5. Experimental Application

5.1. Assembly task

An assembly task has been selected as a case-study task in order to validate the defined control strategies (presenting important issues such as rebounding instabilities, force overshoots, crucial first contact phase).

https://doi.org/10.1017/S0263574716000461 Published online by Cambridge University Press

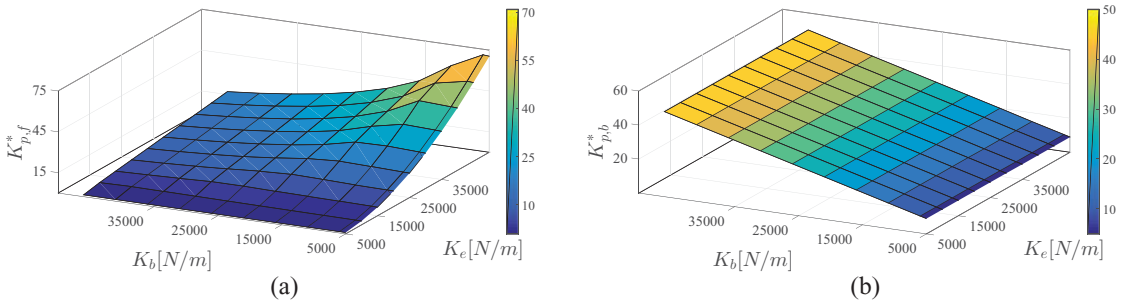

Fig. 4. (a) Map of values of optimal gain $K^{\star}_{p,f}$ given a combination of the stiffness of the robot base K_b and the stiffness of the interacting environment K_e. Single view for robot stiffness $K_r = 1000$ N/m. The closed loop stability is achieved for any combination of robot base and interacting environment. The plot shows that proper values for the proportional gain to be used as the interacting environment becomes softer and the robot base becomes stiffer. (b) Map of values of optimal gain $K^{\star}_{p,b}$ given a combination of the stiffness of the robot base K_b and the stiffness of the interacting environment K_e. Single view for robot stiffness $K_r = 1000$ N/m. The closed loop stability is achieved for any combination of robot base and interacting environment. The plot shows that such optimal gain is almost exclusively a function of the K_b/K_r ratio, while the dependence of the environment stiffness K_e is almost absent.

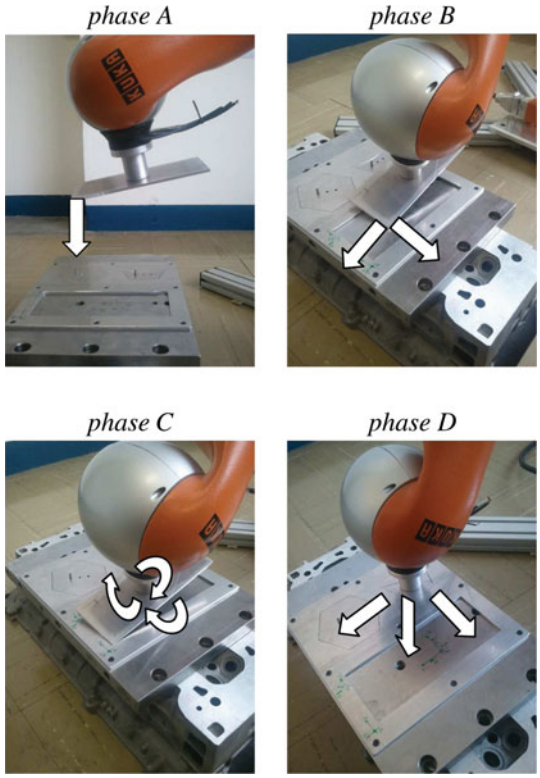

Fig. 5. The defined assembly task phases are shown. *Phase A*: the robot approaches the target environment along Z direction; *Phase B*: the robot explores the translational directions X and Y; *Phase C* rotations are enabled and the assembly task is performed; *Phase D*: the complete set of stiffnesses in the translational directions X, Y and Z is estimated.

In order to execute the selected assembly task, 4 phases are recognized in a very intuitive way (Fig. 5):

Phase A. Approach and contact detection in the vertical direction Z and on-line estimation of $\widehat{K}_{e,z}$ in the vertical direction Z.
Phase B. Exploration along translation components and estimation of $\widehat{\mathbf{K}}_e$. The impedance control set-point $\mathbf{x}_r^0$ and the controlled robot stiffness $\mathbf{K}$ and damping $\mathbf{D}$ are computed

https://doi.org/10.1017/S0263574716000461 Published online by Cambridge University Press

Table I. Global system configurations for the experiments execution.

Config.	Robot	Base-environment
1	soft	soft
2	soft	hard
3	hard	soft
4	hard	hard

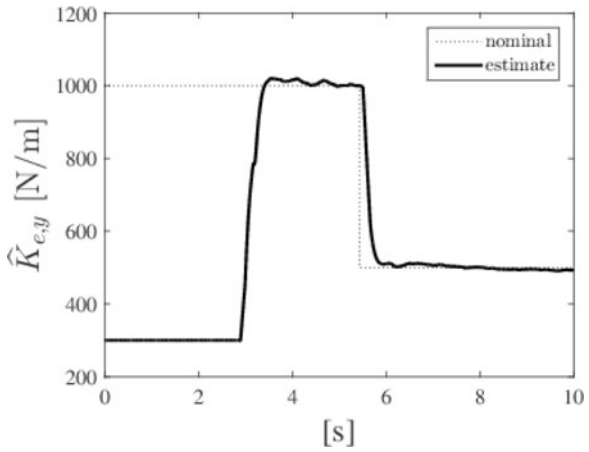

Fig. 6. Stiffness estimation in real experiment in 1 DoF, along a horizontal axis.

as a function of force-tracking error $\mathbf{e}_f = \mathbf{f}^d - \mathbf{f}$ (rotational components of $\mathbf{x}_r^0$ are blocked).

Phase C. Assembly proper, enabling rotations for insertion and relying on $\widehat{\mathbf{K}}_e$ observed along the searching directions. The set-point $\mathbf{f}^d$ enables also torques.

Phase D After tight assembly, on-line estimation of (possibly changing) $\widehat{\mathbf{K}}_e$.

5.2. Observers results

5.2.1. EKF – experimental results. Characterization, tuning and evaluation of the observer in (7) are performed in real experiments for the estimation of the environment stiffness $\widehat{K}_e$, after the localization of the environment location $\mathbf{x}_e^{eq}$.

The on-line estimation of environment stiffness can be executed using the 1-DoF formulation of (6) for the filter states update.

In Fig. 6, a varying stiffness environment is observed (a companion LWR 4+ in impedance control is used to generate a non-shared reference stiffness) in a real experiment. Experimental results show a delay in the estimation of approximately 0.5 s and a maximum steady state error of less than 1% and 3% w.r.t. the known nominal values.

5.2.2. KF - experimental results. Based on the estimated robot base dynamic parameters the KF is implemented and the estimated robot base position is compared with the measurements obtained from validation lasers during a real assembly task with a 2 DoFs robot base.

Experimental results in Fig. 7 show the capabilities of the observer to estimate the robot base position even during transition phases. Differences between lasers measurements and estimates are related to error during the dynamic parameter estimation phase and to the static friction that is not considered in the model.

5.3. Control strategies validation

The experimental set-up used to validate the defined robot base dynamics compensation controller is shown in Fig. 8.

The used manipulator (a KUKA LWR 4+) is mounted on a standard industrial non-actuated mobile platform located close to the assembly area.The mobile platform wheels introduce a compliance in

https://doi.org/10.1017/S0263574716000461 Published online by Cambridge University Press

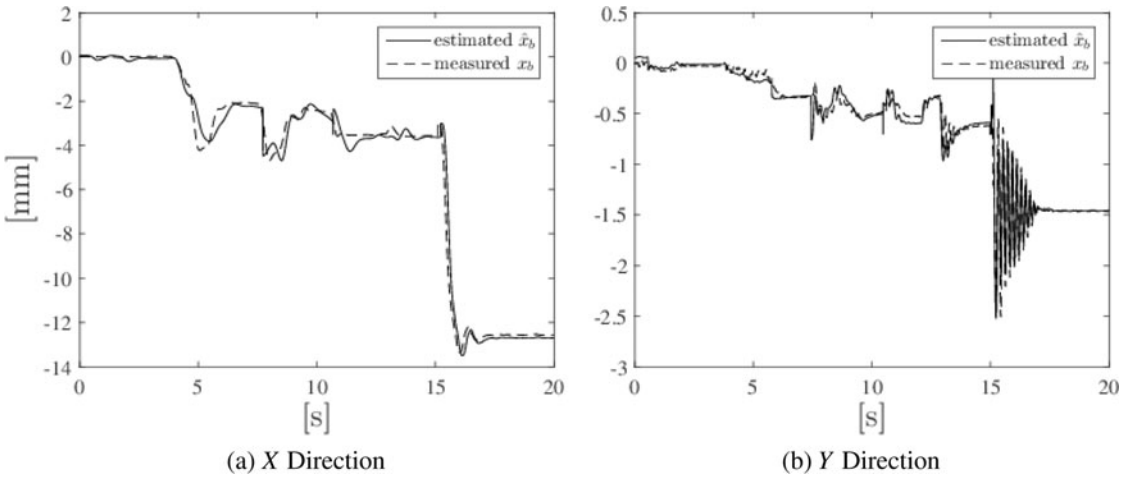

Fig. 7. Robot base position estimation. (a) Soft behavior in X direction is set (≈5000 N/m), (b) hard behavior in Y direction is set (≈50, 000 N/m).

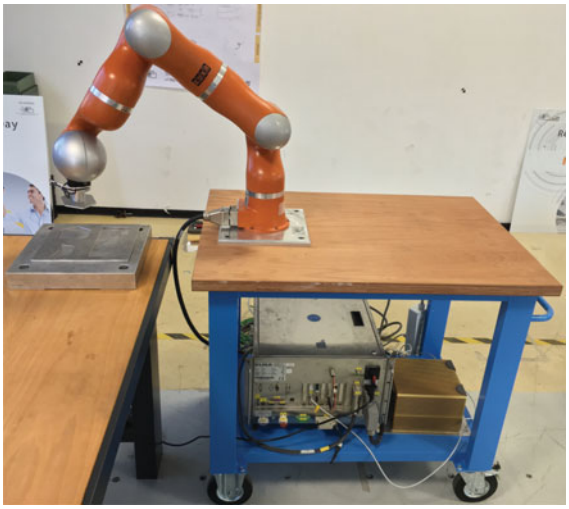

Fig. 8. Compliant KUKA LWR at CNR-ITIA, IRAS group, inserting shapes (unknown to the controller) in interaction with a compliant environment. A standard industrial non-actuated mobile platform has been used as support and wheels introduce compliance in the robot base.

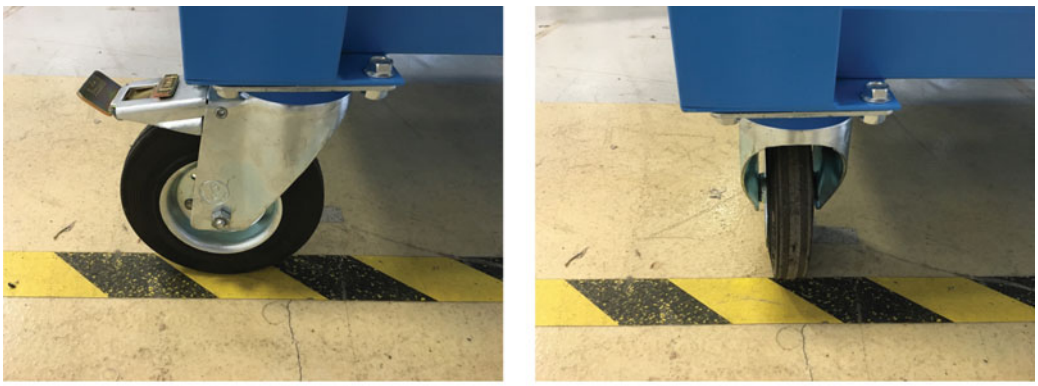

Fig. 9. Compliant robot base wheels configuration. (a) configuration results in a softer equivalent stiffness (5000 N/m), while (b) configuration results in a harder equivalent stiffness (50, 000 N/m) due to both the mechanical structure of the wheel and the tyre configuration (modeling of tyre stiffness is shown in ref. [34]).

https://doi.org/10.1017/S0263574716000461 Published online by Cambridge University Press

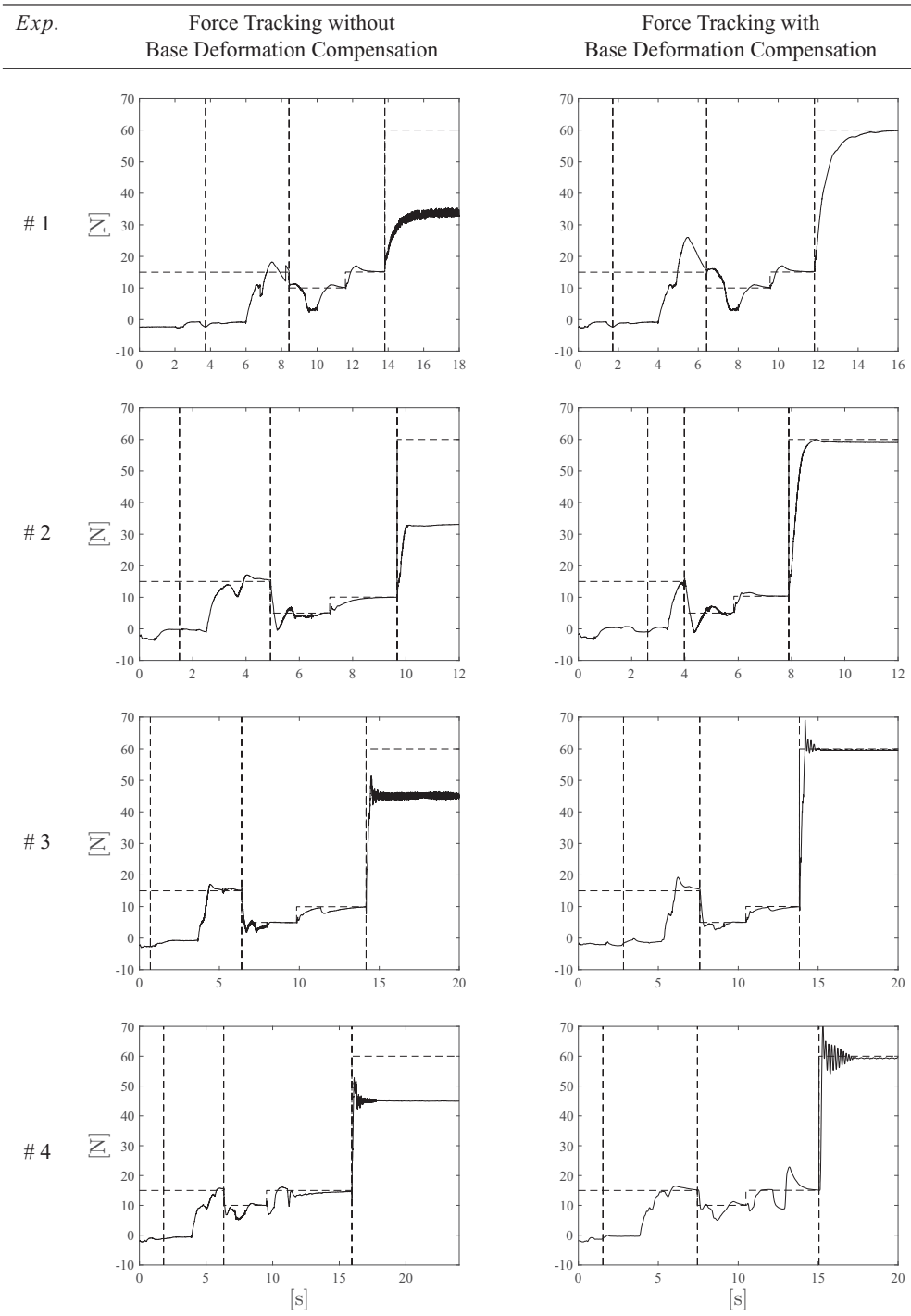

Fig. 10 Interaction force in Y direction. The four phases of the assembly task are highlighted. Reference force (dashed line) and measured force (continuous line) are shown.

the robot base. In particular, it has to be highlighted that the wheels configuration modifies the robot base compliance. In fact, as shown in Fig. 9, by positioning the mobile platform wheels and using the estimation methodology as in Section 3.3, the equivalent robot base stiffness results in 5000 N/m for configuration (a) (without using the mechanical brake) and in 50, 000 N/m (using the mechanical brake). The interaction environment stiffness is varied from succeeding experiments by introducing a compliant layer between the target assembly hole and its grounding. In particular, two different

https://doi.org/10.1017/S0263574716000461 Published online by Cambridge University Press

materials have been used (soft material stiffness equal to 1500 N/m and hard material stiffness equal to 15, 000 N/m). Therefore, four experiments have been carried out using the configurations detailed in Table 5.2.2.

The defined strategy has been compared with a force-tracking controller without robot base dynamics compensation in order to show its better performance. In particular, in order to properly position the component for the final demonstration phase D (final insertion phase) and start in the same operating conditions, phases from A to C were executed using the proposed control schema in all the experiments.

In Fig. 10 the base compensation effect is shown for Y direction (same results are obtained in X direction). In phase A, the robot is moving only in Z direction and no force is measured in Y direction. In phase B, reference force f_y^d is set to achieve smooth first contacts. In phase C, rotations have been commanded to insert the geometry. In phase D, f_y^d is set to 60 N to have a tight assembly of the parts. The task-D execution without base compensation is entirely in charge of the force error gain, resulting in a large steady state error (softer robot bases give rise to higher steady state error since a greater part of the interaction force is absorbed by a greater deformation), while the defined algorithm allows the obtainment of a zero steady state error. However, oscillations are present in the system response as the global system become stiffer. This response is common for proportional controller and it can be damped considering a derivative gain in the control design. The bandwidth of the closed loop system is different in the four experiments (it depends on the dynamics parameters of the coupled dynamics model in (4)). Therefore, as the environment and robot base stiffnesses become higher, the bandwidth of the coupled system increases. Moreover, Fig. 4 shows that higher control gains values can be used for stiffer systems, again increasing the closed-loop bandwidth.

6. Conclusion

Based on force-tracking impedance control laws, a force-tracking control algorithm for compliant mounting robot have been implemented and tested in a full rigid body assembly real task. The developed strategy allows the tracking of a target force during the task execution while compensating for the robot base dynamics, using the estimation of the interacting environment stiffness (EKF) and the estimation of the robot base position (KF).

The method is capable of taking into account the floor properties, by identifying an equivalent compliant system for the robot platform. Such equivalent system dynamics results from both the compliant platform dynamics and from the floor dynamics. In order to properly model the floor dynamics, the compliant platform model can be extended, considering a higher order model.

Experimental results show the proper force tracking (i.e., zero steady state error). Even if a simpler controller can be designed to execute a force tracking task with compliant mobile platform (e.g., PID controller) without any knowledge of the interaction model, the proposed method can be easily applied to any scenario, only executing the fast off-line identification procedure to characterize the compliant platform (in case of any changes in the operating conditions). In fact, a generic controller will need to tune the control gains based on experiments any time the operating conditions change. Moreover, the stability of the system will not be guaranteed.

To improve the control performance, a non-linear model of the robot base is considered for upgrading the estimate, together with the derivative terms in the control loop. Non-linearities in the contact and environment stiffness model would similarly contribute to the overall performance of both force-tracking and impedance models. Moreover, rotations will be taken into account in order to improve the performance during the rotation phase, also updating the contact model in order to take into account the resulting coupling in the degrees of freedom.

Acknowledgment

The authors would like to thank T. Dinon (CNR-ITIA) and F. Paolucci (CNR-ITIA) for expertise and support.

The work has been developed within the project European Robotic Challenge, funded from European Union's Seventh Framework Programme under grant agreement n. 608849.

References

1. E. Colgate and N. Hogan, "The Interaction of Robots with Passive Environments: Application to Force Feedback Control," **In**: *Advanced Robotics: 1989* (Kenneth J. Waldron, ed.) (Springer, 1989) pp. 465–474.
2. E. D. Fasse and N. Hogan, "Control of Physical Contact and Dynamic Interaction," **In**: *Robotics Research* (Georges Giralt Gerhard Hirzinger Prof. Dr.-Ing.) (Springer, 1996) pp. 28–38.
3. J. K. Salisbury, "Active Stiffness Control of a Manipulator in Cartesian Coordinates," *Proceedings of the 19th IEEE Conference on Decision and Control including the Symposium on Adaptive Processes,*, IEEE, Stanford, CA, USA, vol. 19 (Dec. 1980) pp. 95–100.
4. M. T. Mason, "Compliance and force control for computer controlled manipulators," *IEEE Trans. Syst. Man Cybern.* **11**(6), 418–432 (1981).
5. M. H. Raibert and J. J. Craig, "Hybrid position/force control of manipulators," *J. Dyn. Syst. Meas. Control* **103**(2), 126–133 (1981).
6. T. Yoshikawa, "Dynamic hybrid position/force control of robot manipulators–description of hand constraints and calculation of joint driving force," *IEEE J. Robot. Autom,* **3**(5), 386–392 (1987).
7. O. Khatib, "A unified approach for motion and force control of robot manipulators: The operational space formulation," *IEEE J. Robot. Autom.* **3**(1), 43–53 (1987).
8. N. Hogan, "Impedance Control: An Approach to Manipulation," *American Control Conference, 1984* (Jun. 1984) pp. 304–313.
9. E. Colgate and N. Hogan, "An Analysis of Contact Instability in Terms of Passive Physical Equivalents," *Proceedings of the IEEE International Conference on Robotics and Automation (ICRA)*, IEEE (1989) pp. 404–409.
10. L. Roveda, F. Vicentini and L. Molinari Tosatti, "Deformation-Tracking Impedance Control in Interaction with Uncertain Environments," *Proceedings of the IEEE/RSJ International Conference on Intelligent Robots and Systems (IROS)*, IEEE (2013) pp. 1992–1997.
11. R. Volpe and P. Khosla, "The equivalence of second-order impedance control and proportional gain explicit force control," *Int. J. Robot. Res.* **14**(6), 574–589 (1995).
12. L. Villani, C. Canudas de Wit and B. Brogliato, "An exponentially stable adaptive control for force and position tracking of robot manipulators," *IEEE Trans. Autom. Control* **44**(4), 798–802 (1999).
13. H. Seraji and R. Colbaugh, "Adaptive Force-Based Impedance Control," *Proceedings of the 1993 IEEE/RSJ International Conference on Intelligent Robots and Systems' 93, IROS'93*, Yokohama, Japan, vol. 3, IEEE (1993) pp. 1537–1544.
14. H. Seraji and R. Colbaugh, "Force tracking in impedance control," *Int. J. Robot. Res.* **16**(1), 97–117 (1997).
15. S. Jung, T. Hsia and R. Bonitz, "Force tracking impedance control of robot manipulators under unknown environment," *IEEE Trans. Control Syst. Technol.* **12**(3), 474–483 (2004).
16. K. Lee and M. Buss, "Force tracking impedance control with variable target stiffness," *Int. Fed. Autom. Control* **16**(1), 6751–6756 (2000).
17. S. Oh, H. Woo and K. Kong, "Frequency-shaped impedance control for safe human–robot interaction in reference tracking application," *IEEE/ASME Transactions on Mechatronics* **19.6**, 1907–1916 (2014).
18. M. Torres and S. Dubowsky, "Path-Planning for Elastically Constrained Space Manipulator Systems," *Proceedings of the IEEE International Conference on Robotics and Automation*, IEEE International Conference, vol. 1 (1993) pp. 812–817.
19. C. Wronka and M. Dunnigan, "Derivation and analysis of a dynamic model of a robotic manipulator on a moving base," *Robot. Auton. Syst.* **59**(10), 758–769 (2011).
20. K. Yoshida, D. Nenchev and M. Uchiyama, "Moving Base Robotics and Reaction Management Control," **In**: *Robotics Research* (G. Giralt and G. Hirzinger, eds.) (Springer, London, 2000) pp. 100–109.
21. J. Y. Lew and S.-M. Moon, "A simple active damping control for compliant base manipulators," *IEEE/ASME Trans. Mechatronics* **6**(3), 305–310 (2001).
22. J. Lew, "Contact Control of Flexible Micro/Macro-Manipulators," *Proceedings of the IEEE International Conference on Robotics and Automation, 1997*, Albuquerque, New Mexico, vol. 4 (1997) pp. 2850–2855.
23. C. Ott, A. Albu-Schaffer and G. Hirzinger, "A Cartesian Compliance Controller for a Manipulator Mounted on a Flexible Structure," In: *Proceedings of the IEEE/IROS International Conference on Intelligent Robots and Systems*, IEEE, RSJ, Beijing (2006) pp. 4502–4508.
24. T. Wongratanaphisan and M. Cole, "Robust impedance control of a flexible structure mounted manipulator performing contact tasks," *IEEE Trans. Robot.* **25**(2), 445–451 (2009).
25. A. Albu-Schäffer, C. Ott and G. Hirzinger, "A unified passivity-based control framework for position, torque and impedance control of flexible joint robots," *Int. J. Robot. Res.* **26**(1), 23–39 (2007).
26. L. Roveda, Model Based Compliance Shaping Control of Light-Weight Manipulator in Hard-Contact Industrial Applications, Ph.D. dissertation (Politecnico di Milano, Mechanical Engineering Department, Italy, 2015).
27. W. Flügge, *Viscoelasticity* (Springer, New York, 1975).
28. P. R. Kraus and V. Kumar, "Compliant Contact Models for Rigid Body Collisions," In: *Proceedings of the IEEE International Conference on Robotics and Automation*, IEEE, Albuquerque, New Mexico, vol. 2, 1997, pp. 1382–1387.
29. M. K. Vukobratović and V. Potkonjak, "Dynamics of contact tasks in robotics. Part I: general model of robot interacting with environment," *Mech. Mach. Theory* **34**(6), 923–942 (1999).

30. D. N. Nenchev, K. Yoshida, P. Vichitkulsawat and M. Uchiyama, "Reaction null-space control of flexible structure mounted manipulator systems," *IEEE Trans. Robot. Autom.* **15**(6), 1011–1023 (1999).
31. M. Weber, O. Ma and I. Sharf, "Identification of Contact Dynamics Model Parameters from Constrained Robotic Operations," *Proceedings of the ASME International Design Engineering Technical Conferences and Computers and Information in Engineering Conference. Montreal, Canada, ASME* (2002) pp. 1289–1298.
32. S. S. Haykin *et al.*, *Kalman Filtering and Neural Networks* (Wiley Online Library, New Jersey, 2001).
33. J. S. Bendat and A. G. Piersol, *Random Data: Analysis and Measurement Procedures*, vol. 729 (John Wiley & Sons, New Jersey, 2011).
34. M. H. R. Ghoreishy, "A state of the art review of the finite element modelling of rolling tyres," *Iran. Polym. J.* **17**(8), 571–597 (2008).

https://doi.org/10.1017/S0263574716000461 Published online by Cambridge University Press